Intersection of a Sloping Aerosol Layer Observed by Airborne Lidar with a Cloud-Capped Marine Boundary Layer

R. L. SCHWIESOW, S. D. MAYOR,* V. M. GLOVER AND D. H. LENSCHOW

National Center for Atmospheric Research,† Boulder, Colorado.

(Manuscript received 12 March 1990, in final form 18 June 1990)

ABSTRACT

The NCAR Airborne Infrared Lidar System (NAILS) observed the edge of an extended, sloping aerosol layer that intersected a stratocumulus cloud deck over the Pacific Ocean during the First ISCCP (International Satellite Cloud Climatology Project) Regional Experiment, 260 km WNW of San Diego. In situ measurements support the interpretation of the lidar observations as arising from a particle-laden layer with relatively clean air above, below, and to the SW. Intersection of these sloping layers with cloud top leads to substantial horizontal variability of boundary-layer structure in the intersection region. The intersection of the aerosol layer with cloud top also corresponded closely to a quasi-linear trough in the cloud top that showed enhanced brightness and an enhanced number of small particles.

1. Introduction

The first operational use of the NCAR Airborne Infrared Lidar System (NAILS) (Schwiesow 1987) occurred during the First ISCCP (International Satellite Cloud Climatology Project) Regional Experiment (FIRE-Stratocumulus) (Albrecht et al. 1988) in the summer of 1987. The system was mounted in the NCAR Electra and was used both for upward- and downward-looking measurements of cloud edge. Here we discuss a particular case on 16 July 1987 when a sloping aerosol layer was detected while flying just upwind of San Nicholas Island 260 km WNW of San Diego. The airplane was above the low-level stratocumulus clouds with the NAILS looking down. Our observations are related to the study on the same day made by Paluch et al. (1989) who also analyzed the Electra aircraft data.

The purposes of this paper are 1) to illustrate the utility of lidar in displaying the structure of a layered atmosphere, including the ability to locate particle-laden air masses (or assure their absence) for atmospheric chemical measurements; 2) to add to the body of information on elevated aerosol layers by describing remotely sensed observations in a vertical plane above a solid cloud deck; and 3) to document some aspects of horizontal variability in and above stratiform cloud layers and show how linear features in the top of such layers may result from interaction with sloping aerosol layers.

Because the lidar can be used to produce images in a vertical plane on the meteorological microscale, it provides a different class of data than is available from airborne in situ probes, which can give information only along a line. Such observations are not new. Uthe et al. (1980) and Browell et al. (1983), for example, describe lidar observations of aerosol layers above the boundary layer, and Melfi et al. (1985) and Boers et al. (1988) describe lidar observations of stratocumulus cloud top structure. This is, however, the first example we are aware of that involves the intersection of an aerosol layer in the overlying free atmosphere with a stratocumulus cloud deck, with documentation of the relevant atmospheric structure by in situ measurements from a well-instrumented research aircraft.

The observation, first made by the NCAR Electra pilots, of a quasi-linear trough in the solid stratocumulus cloud top that appeared abnormally bright prompted us to examine closely the lidar backscatter profiles in the region of the feature. At the time of the observation, the aircraft was at an altitude of 1550 m, approximately 760 m above the cloud, which had tops at 790 ± 50 m mean sea level (MSL). The feature, which could be seen from horizon to horizon with some gentle curvature, was estimated by eye to be between 100 m and 1 km wide. Figure 1 shows a pair of similar features from another research flight over marine stratocumulus in the same general area. No equivalent photographs are available from this flight. This type of feature is known by aircraft observers who have participated in this and other experiments to occur fre-

* *Current affiliation:* ST Systems Corporation, Hampton, VA 23666.

† The National Center for Atmospheric Research is sponsored by the National Science Foundation.

Corresponding author address: Dr. Ronald L. Schwiesow, National Center for Atmospheric Research, P.O. Box 3000, Boulder, CO 80307-3000.

FIG. 1. Photograph of the top of a marine stratocumulus layer (different from the one discussed here, but in the same general area and same time of year) showing two bright quasi-linear features similar to the one analyzed here.

quently in areas with solid marine stratocumulus cloud cover.

We make the case here that the observed feature is associated with the intersection of a sloping layer in the free atmosphere with the cloud top. This layer is characterized by enhanced aerosol concentration. The visual appearance of both the cloud top feature and the lidar cross section of the aerosol layer above cloud suggested to us initially that the feature might have resulted from some inherently linear process such as the exhaust plume from a ship passing through the area. For example, Radke et al. (1989) documented effects on cloud microphysics caused by ship exhaust in this same general area during FIRE. Plume rise energetics, however, rule out the possibility that a ship plume could have penetrated the extremely stratified layers above the cloud.

2. Lidar observations

a. Vertical cross section

Figure 2 shows relative backscattering observed on a time-height display from the downward-pointing lidar. Note that the layer containing increased particulate loading descends along the flight track from B, where it first appears below the aircraft at the minimum system range, to C, where it is completely engulfed in the cloud-capped mixed layer. This leg of the flight was at a constant altitude of 1550 ± 10 m. (The increased distance between the lidar and cloud top before B is caused by aircraft roll in a turn.) Note also the relatively clean layer (i.e., lower particle concentration) immediately above the cloud just before C.

The gray scale in Fig. 2 indicates relative backscatter intensity corrected for the range-squared factor in the lidar equation (e.g., Schwiesow 1987). The backscatter cross section is limited on the top by the tail of the transmitted laser pulse and on the bottom by the cloud, which was dense enough in this case that it was not penetrated by the lidar pulse. Times are given in UTC; subtract eight hours for local standard time.

For these observations, we used a lidar based on a CO_2 laser operating at a wavelength of 10.6 μm (Schwiesow 1987; Schwiesow et al. 1988). The effective range resolution (the ability to distinguish two separated features) for weak (aerosol) scattering was approximately 30 m. For strong scatterers, such as the cloud, the range resolution was degraded to as much as 250 m because the relatively weaker scattered intensity at a given altitude from the tail of the laser pulse

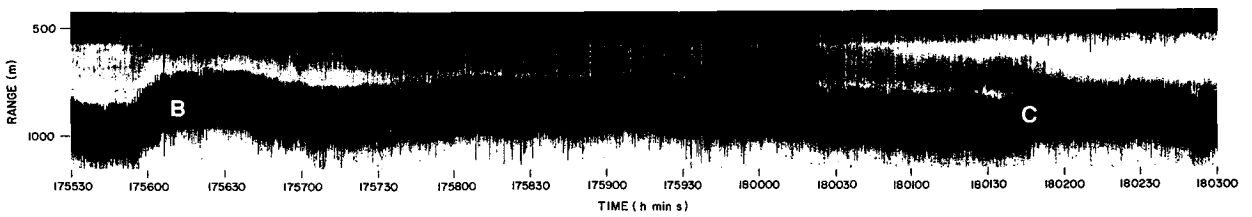

FIG. 2. Backscatter cross section in gray scale as a function of time, which is proportional to distance along the flight track. The lower black layer is cloud, the white regions are clear air and the gray region is the aerosol layer. The black region at the top is the tail of the transmitted pulse. Points B and C in time are located approximately 42 km apart on the flight track plot of Fig. 3, which translates to approximately 7 km per minute on the time axis.

overlapped the return from the leading edge of the pulse at a greater range. The reason for this difference in resolution is that the laser pulse shape consisted of a sharp initial spike of approximately 200 ns duration between half-power points followed by a long, flat tail of slightly less than 2 μs duration and a peak power one-third that of the spike. For weak scatterers, the return from the tail was below the system noise floor, whereas for strong scatterers the return from the tail was detectable and degraded the resolution. The range accuracy (the ability locate the edge of the cloud) was better than the range resolution for strong scatterers; the accuracy was ± 3 m under good conditions. Four profiles per second were recorded, giving a spacing of approximately 30 m along the flight track between profiles. Occasional profiles show weak scattering in the cloud because of laser pulse energy fluctuations. A lidar at a wavelength of 10.6 μm is most sensitive to particles with radii of 1–3 μm for typical continental particle size distributions (Post 1978), so we expect that the return from the scattering layer was from particles of radius $\geqslant 1$ μm.

b. Geometry

The flight track in the region of the intersection of the sloping aerosol layer with the top of the stratocumulus deck is shown in Fig. 3. The series of NE and SW flight tracks was initiated by the turn at point A. The lidar profiles were taken along a southwesterly heading from point B to C. At point C the flight track passed over the linear feature in the cloud top, which is indicated as a dashed line. Winds at flight level along B to C were from 276° at 6.5 m s^{-1}. During the turn at the southwest end of the track, the aircraft descended to cloud top. The aircraft then alternately descended into and ascended out of cloud along a northeasterly heading. This flight track was designed to give high-resolution vertical profiles in the vicinity of cloud top as the aircraft headed toward and through point D, which is the region containing the quasi-linear cloud feature.

Our interpretation of the lidar data in the context of this geometry is that there existed in the region of the observations a sloping aerosol layer with enhanced particulate concentration. Where this layer intersected the cloud top, a line of enhanced brightness occurred. The brightness could be caused by modification of the microphysical processes along the line of intersection, by sun angle on the trough in cloud top, or a combination of these. Relatively clean air existed above the layer and to the southwest of the line of intersection; the particulate-laden layer is above and to the right in Fig. 3. The increased particle concentration in the layer was not noted visually during the flight, probably because it was too thin to provide sufficient contrast against the background clouds.

3. Supporting observations

In order to help understand the lidar observations, and relate them to atmospheric structure, we have an-

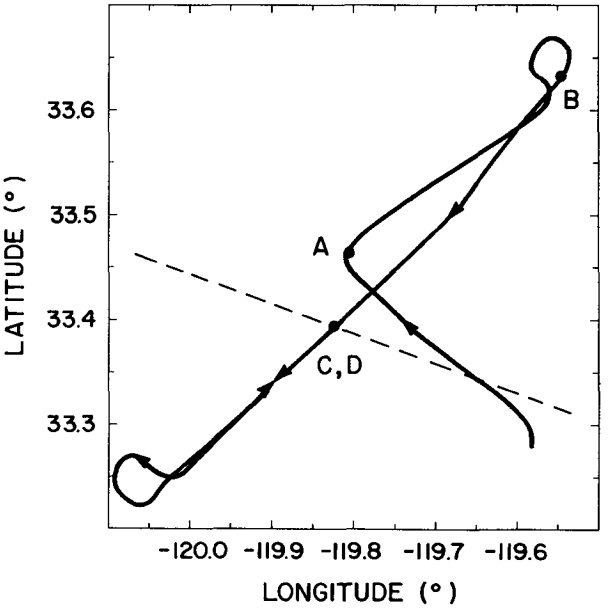

FIG. 3. Flight track in plan view during observations of the sloping aerosol layer and its intersection with the stratocumulus cloud. The quasi-linear feature at cloud top is shown as a dashed line. Observations from B (1756:10 UTC) to C (1801:45 UTC), and near D (1811:35 UTC), which is at the same horizontal position as C but at a height of 790 m instead of 1550 m, are discussed in the text.

alyzed other data from the aircraft, both on the flight leg above the cloud top trough and on the leg flown at cloud top. These data include radiometric temperature and cloud height from B to the turn; temperature and specific humidity profiles during the descending turn; and wind, temperature, specific humidity, and microphysical parameters during the up-and-down flight leg at cloud top.

a. Cloud height and radiation data

We observed that on the leg above cloud the radiometric temperature, as measured by a downward-looking Barnes Engineering PRT-5 radiometer, is sometimes negatively correlated with cloud top height (although with no consistent lapse rate). In Fig. 4 this is true to the left of the arrow marking approximately 1801:45 UTC (point C in Figs. 2 and 3) when the aircraft passed over the intersection of the sloping aerosol layer with the cloud deck. To the right, the radiometric temperature drops sharply by more than one degree. Later we will interpret this change using temperature data from the up-and-down flight leg at cloud top.

The cloud height trace in Fig. 4 shows a dip as the lidar passed over the intersection region at cloud top. This is consistent with the pilots' observations, which characterized the feature as a trough. There is nothing exceptional per se about this dip compared to other nearby dips in cloud height. The exceptional characteristic is the observed horizon-to-horizon extent of the trough transverse to the flight path. Other dips are associated with mesoscale and cloud convective scale structures, which do not extend for more than a few kilometers and are much more sinuous. As indicated in Fig. 4, the cloud top height is approximately the same on both sides of the trough. This is further documented in Fig. 7c, which is discussed as part of the data from the up-and-down flight leg at cloud top.

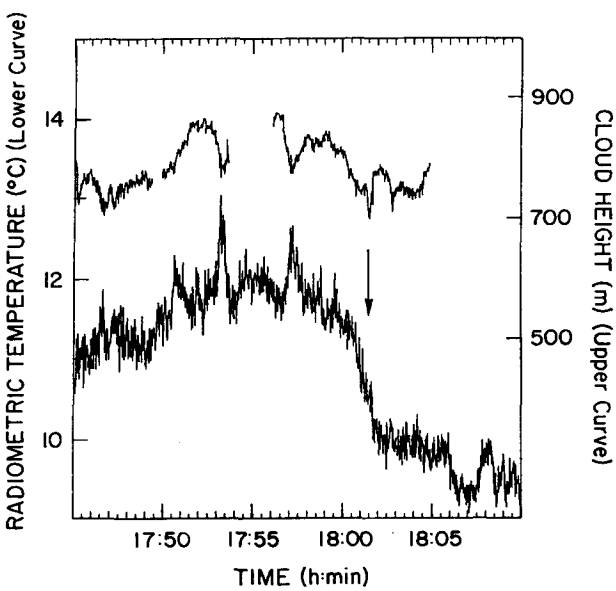

FIG. 4. Cloud top height as measured by the NAILS and radiometric temperature. Blanks in the cloud height trace are from aircraft turns where the lidar range to cloud does not indicate cloud height. The arrow marks the location of the linear feature in the cloud top (point C in Figs. 2 and 3).

Video imagery taken with cameras pointing forward and to either side also showed the linear feature. Unfortunately, the contrast in the video playback was too low to allow successful reproduction of a single frame for publication. Although the hemispherical shortwave radiometer on the Electra has very coarse horizontal resolution from this altitude, it showed a peak of 640 W m^{-2} at 1801:45 UTC as the aircraft passed over the bright feature. Before the trough at 1800:00 UTC the upwelling radiation was approximately 400 W m^{-2}, and at 1802:50 in the cleaner air to the southwest of the trough it was 525 W m^{-2}.

b. Layering

Vertical soundings of potential temperature θ and specific humidity (from a dewpoint hygrometer) q, obtained during the descent from 1500 m to 700 m in the clean air at the southwest end of the flight track (see Fig. 3) are plotted in Fig. 5. We have not removed any offset in θ or q that would be required to give saturation in the cloud layer and below saturation elsewhere. Both θ and q show a well-mixed layer below approximately 800 m. A strong temperature inversion and decrease in humidity occur just above the mixed layer. Additional well-defined layers are evident in the q profile. Just above cloud top, a layer of dry air occurs, which is overlain by a more moist layer. The main decrease in q occurs at an altitude of $\sim$1100 m.

The Particle Measuring Systems active scattering aerosol spectrometer probe (ASASP) measures number concentration of particles with radii between 0.1 and 3.0 μm. Particle concentration was almost constant for the profile in clean air, varying smoothly from approximately 750 cm^{-3} at an altitude of 800 m to 1000 cm^{-3} at 1500 m.

c. Variability at cloud top

The lidar data indicate that the quasi-linear trough observed at cloud top coincides with the intersection of an aerosol layer with cloud top. This means that the air on either side of the intersection came from different layers; therefore we would expect that the structure of the atmosphere would show considerable horizontal variation at cloud top. In interpreting the data from the up-and-down flight leg at cloud top that crosses this trough, it may be helpful to refer to Fig. 6, which is a schematic view of a vertical cross section containing the flight track at two different altitudes, roughly perpendicular to the cloud top trough. Some of the variation in differences between successive peaks and val-

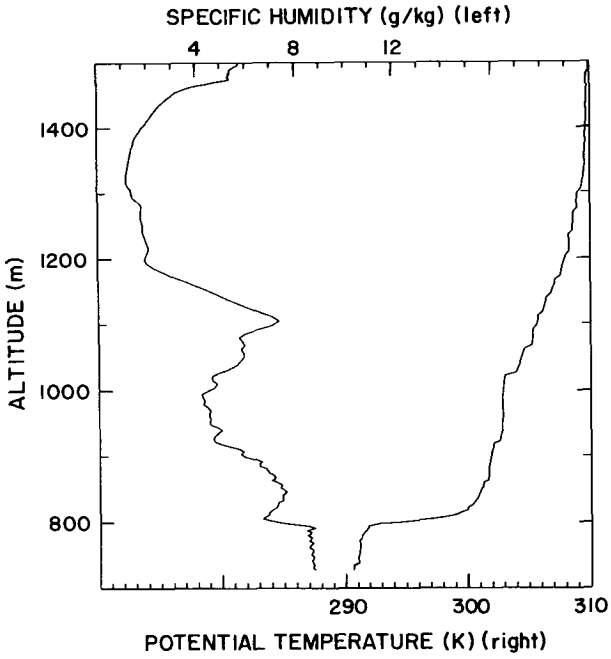

FIG. 5. Profiles of potential temperature and specific humidity through and above the cloud deck taken during the turn at the southwest end of the flight track in Fig. 3.

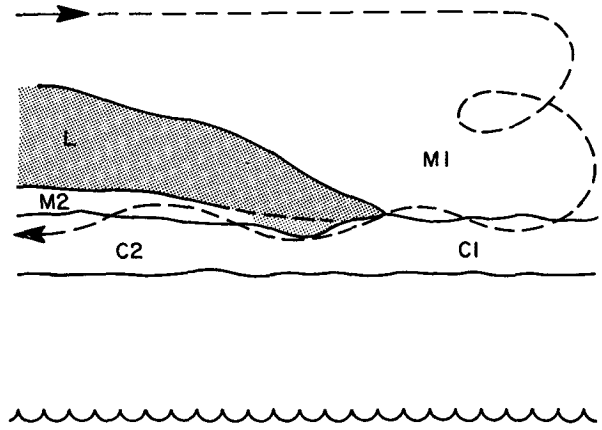

FIG. 6. Schematic illustration of a vertical section through the sloping aerosol layer L and the cloud deck, which is divided into regions $C1$ and $C2$ on either side of the intersection region. The vertical section is approximately perpendicular to the quasi-linear feature in cloud top. Clear layers $M1$ and $M2$ that sandwich L are also shown. The aircraft flight track (see Fig. 3 for plan view) is shown dashed.

leys on the up-and-down leg may be caused by the different heights of the excursions. However, sampled differences are representative of the general features near the trough. The aerosol layer in Fig. 6 is denoted by L. Layers of relatively clean air above and below L and above the cloud layer are denoted by $M1$ and $M2$, and cloud layers on either side of the trough are denoted by $C1$ and $C2$. Increasing time in the time series data corresponds to movement from right to left on the up-and-down leg near cloud top.

Specific humidity q, obtained from a dewpoint hygrometer, exhibits striking horizontal variability in the region of the intersection just above cloud. Figure 7a shows that at peak 1 q is $\sim$6 g kg^{-1}, about the same value as in the sounding just above cloud (Fig. 5). From peaks 2 to 5, which are in the cleaner air SW of the aerosol layer, q increases dramatically to >10 g kg^{-1}; then between peaks 5 and 6, which is where the aerosol layer intersects cloud top (point D in Fig. 3, at 1811:35 $\pm$ 00:10 UTC), q decreases to about 10 g kg^{-1}. From peaks 6 to 11, q continues to decrease, but more slowly, to about 9 g kg^{-1}. Thus, the picture that emerges is that a moist layer of air overlies the aerosol layer. Furthermore, we note a double-peak structure at peaks 2 to 5, which indicates that this moist layer is only $\sim$40 m deep.

Although the dewpoint hygrometer may not be accurate in cloud, we note that specific humidity in the cloud increases gradually from $\sim$8.5 g kg^{-1} between peaks 3 and 4 to about 10 g kg^{-1} beyond peak 11, consistent with the observed increase in temperature. Since the liquid water is never greater than about 0.3 g kg^{-1}, the same conclusion holds for total water mixing ratio. The picture that emerges is a sloping layer of moist air with a total water concentration being greater above cloud than within cloud in the region where this layer intersects the inversion.

Potential temperature exhibits a less dramatic change between different layers in Fig. 7b. The air above the cloud deck at about the same height ($\sim$840 m MSL) is approximately 1°K warmer on the clean side of the trough than it is on the side of the intersection under

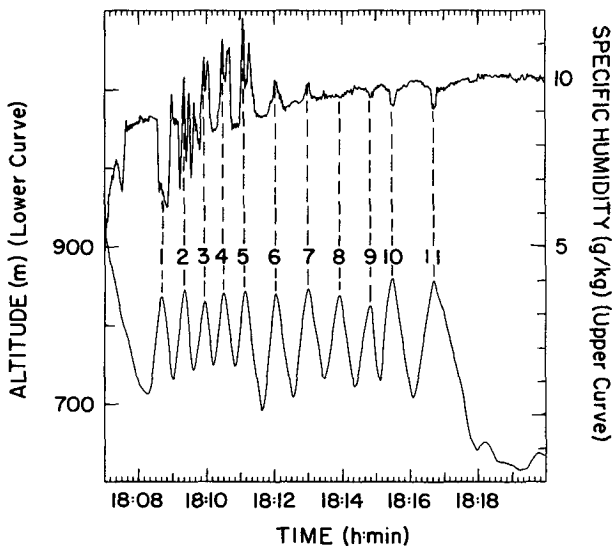

FIG. 7(a). Altitude and specific humidity near cloud top. The altitude peaks are referred to in the text by numbers 1 through 11 from left to right. The trough in cloud top is between peaks 5 and 6.

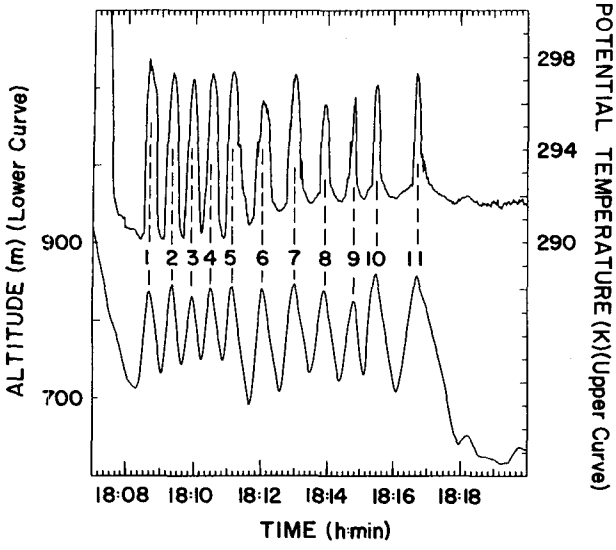

FIG. 7(b). As in Fig. 7(a) except with potential temperature.

the aerosol layer. (This temperature difference is obtained at a constant altitude, and not at a constant height above the inversion at cloud top, which, as shown in Fig. 7c, varies in height across this region.) On the other hand, the temperature in the cloud is approximately 2°K warmer on the aerosol side of the line, which means that the jump in temperature across the inversion changes from ~7°K SW of the trough to ~4°K NE of the trough. The jump in liquid-water potential temperature (a variable that is conserved with respect to phase changes) across the inversion changes from ~8°K SW of the trough to ~5°K NE of the trough.

The radiative temperature verifies that the cloud top as seen from above is approximately 2°K warmer for the cloud under the aerosol layer (to the northeast in Fig. 3). Although not shown here, the radiative temperature seen at the bottom of the dips in the cloud (to an altitude of 730 m) on the aerosol side of the trough increases by one to two degrees more than what would be expected solely from a wet-adiabatic sounding through cloud. This indicates that a significant fraction of the radiometer signal is coming from the warmer sea surface, which is a consequence of thinner cloud or higher cloud base NE of the trough. The suggestion of a thinner cloud (or differences in droplet size distribution) is supported by the upwelling shortwave radiation measured above cloud, which is less under the aerosol layer than it is on the SW side of the trough. Upward radiation of 580 ± 50 W m^{-2} on the clean side of the trough drops to 350 ± 100 W m^{-2} under the aerosol layer. These values and their differences are similar to those measured from an altitude of 1550 m MSL during the overflight described earlier.

Liquid water was measured with a King hot-wire probe. Double peaks in the liquid-water density as shown in Fig. 7c indicate a maximum in liquid water (up to 0.3 g m^{-3}) near cloud top, decreasing through the cloud. Although the liquid-water density is approximately the same on both sides of the intersection, there is a horizontal variation in content toward and away from the minimum between peaks 5 and 6. Note that for the dip into cloud between 5 and 6 the aircraft descended below 700 m, and that the liquid-water density was comparatively small there. This decrease in cloud-top height of approximately 50 m near the location of the linear feature is consistent with the lidar measurements in Fig. 4.

Independent measurements of liquid water by integrating the Particle Measuring Systems forward scattering spectrometer probe (FSSP) particle data showed roughly the same values as Fig. 7c before the dip but showed maxima of ~0.2 g m^{-3} for the cloud after the dip, under the enhanced aerosol layer. The average particle diameter changed from ~18 μm under the clean air to ~12 μm under the enhanced aerosol layer.

The concentration of particles measured with the FSSP (0.5 to 45.0 μm diameter) varied with location along the flight track almost exactly as the liquid-water concentration did. Particle concentrations went from 0 above the cloud to 80 cm^{-3} in denser parts of the cloud. The concentration of these particles in the cloud reached a relative minimum of approximately 30 cm^{-3} between altitude peaks 5 and 6.

In striking contrast to the minimum in large particle concentration between peaks 5 and 6, the small-particle concentration measured by the ASASP (0.1 to 3.0 μm diameter) probe jumped from less than 1000 cm^{-3} to over 6000 cm^{-3} for only this particular dip into the

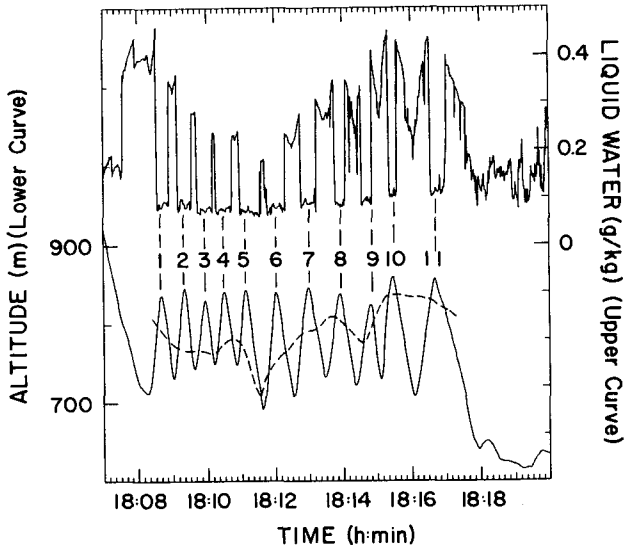

FIG. 7(c). As in Fig. 7(a) except with liquid water. Double peaks are discussed in the text. The zero liquid water baseline is offset by approximately 0.1 g kg^{-1}. Approximate cloud top is indicated by the dashed line. The variation in the concentration of large cloud droplets was very similar to the trace for liquid water.

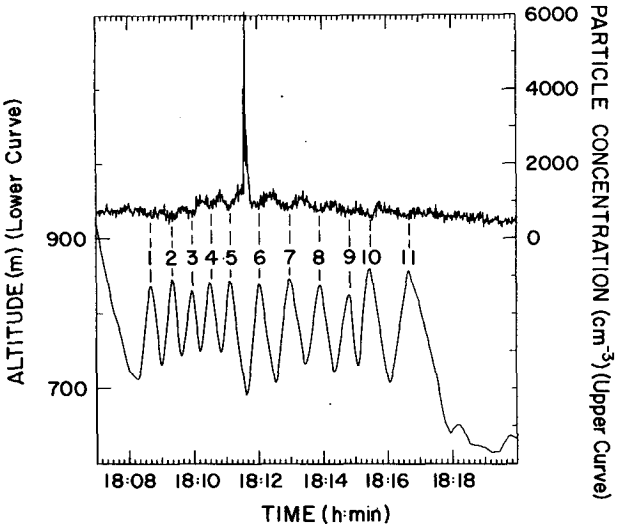

FIG. 7(d). As in Fig. 7(a) except with small particle concentration measured with the ASASP. The concentration shows a single penetration of the aerosol layer at the location of the linear feature in the cloud top.

cloud deck. These data in Fig. 7d clearly locate the intersection of the aerosol layer with cloud top between altitude peaks 5 and 6 and establish that the intersection zone is approximately 1 km wide (concentration spike 10 s times flight speed of approximately 100 m s^{-1}). Furthermore, the particle concentration is larger in cloud than above cloud on both sides of the maximum between peaks 5 and 6. This enhancement dies away on both sides of the peak. Measurements of CO concentration showed a maximum that coincided with the maximum of small particles.

The mean diameter of the particles measured by the ASASP increased rather smoothly through the transition zone, from 0.17 μm at the left of Fig. 7d to 0.19 μm at the right. At the strong peak in concentration in the enhanced aerosol layer, the mean diameter was 0.20 μm. We can dismiss the possibility that the large number of particles in cloud resulted from large values of supersaturation that could occur in regions of large updraft, since the vertical wind was -0.1 m s^{-1} with fluctuations $< \pm 0.1$ m s^{-1} between peaks 3 and 9.

The horizontal variability of ozone in Fig. 7e is similar to that of temperature. Above the cloud on the clean side of the trough the ozone mixing ratio is significantly larger than on the side under the aerosol layer. On the other hand, in cloud the concentration is ~30 ppbv on the clear side of the trough and ~50 ppbv on the aerosol side. As a result, the jump in ozone across cloud top changes from ~120 ppbv SW of the trough to ~30–90 ppbv NE of the trough. The double concentration peaks on the left in Fig. 7e indicate, as for q, that the ozone concentration reaches a maximum in a thin layer just above cloud top. The ozone concentration below the aerosol layer NE of the trough is considerably lower than near the trough. Again, as with q, within these larger-scale changes in ozone, significant smaller-scale structure exists, so that considerable horizontal variability occurs, even on scales of a few kilometers.

In addition to large changes in scalar quantities in the region of the trough, the horizontal wind changed substantially from one side of the trough to the other, both in the cloud and in the air above. Figure 7f shows the wind speed in the air above the cloud deck gradually changing from less than 2 m s^{-1} at altitude peaks 1–5 to approximately 7 m s^{-1} by peak 9. The horizontal gradient of wind speed is even larger in the cloud than above. In cloud, the speed changes from less than 1 m

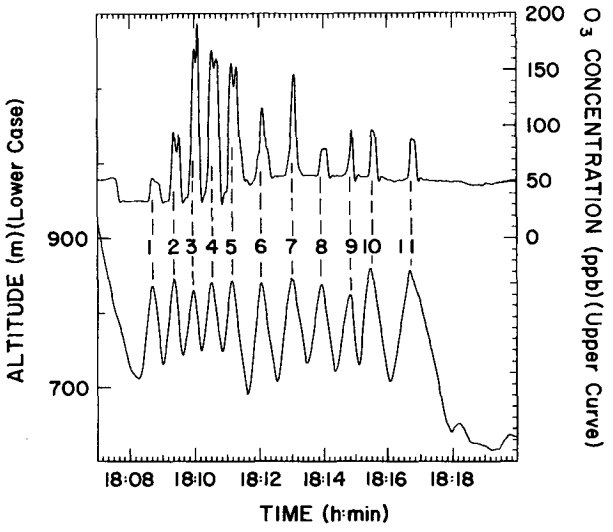

FIG. 7(e). As in Fig. 7(a) except with ozone mixing ratio.

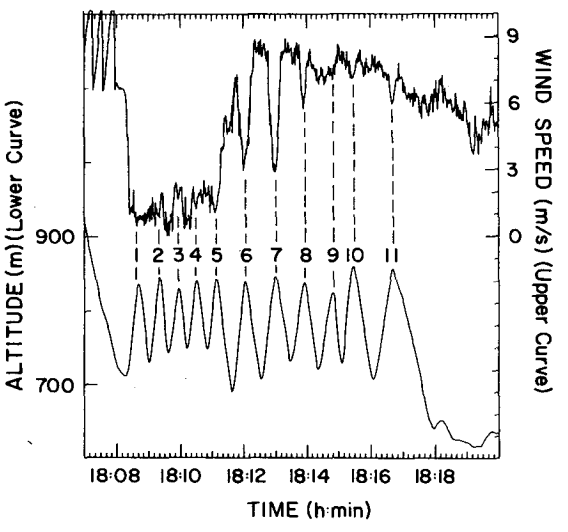

FIG. 7(f). As in Fig. 7(a) except with wind speed.

s^{-1} before peak 4 to greater than 8 m s^{-1} after peak 6. The transition between wind regimes in cloud occurs near the intersection of the aerosol layer with the cloud deck as shown in Fig. 7d, but the largest transition in speed above cloud is well to the NE of the aerosol layer, between peaks 7 and 9. The wind direction above cloud, shown in Fig. 7g, veers from ~100° at peak 1 to ~160° at peak 4, then backs to ~100° after that. Within the cloud, the wind veers from ~220° between peaks 1 and 2 to ~300° between peaks 3 and 4, then backs to ~100° after that. Obviously, the trough location marks not only a significant change in scalar variables in cloud, but also in the horizontal wind field. Furthermore, NE of the trough, where the wind speed is significant, the flow is roughly parallel to the trough.

In the sections of the time series between peaks 5 and 8 where the airplane is just above cloud top, the wind shear is large enough that the gradient Richardson number, $\mathrm{Ri} = g\Theta^{-1}\Delta\theta\Delta z/[(\Delta u)^2 + (\Delta v)^2]$, is <0.5. This brings up the possibility of turbulence generation by shear-driven instabilities, and consequently an enhanced entrainment (and detrainment) rate in this region. The vertical velocity time series bears out this expectation, in showing enhanced fluctuations just above cloud top in the region between peaks 5 and 8 compared to the cloud-top region associated with the other peaks.

4. Summary and interpretation of results

A vertical cross section of lidar backscatter from aerosols measured from an aircraft over the eastern Pacific gives evidence for a sloping aerosol layer intersecting a stratocumulus cloud deck. At the intersection, a quasi-linear trough in cloud top was noted visually. Small-particle concentration in the vicinity of the trough supports this interpretation. In situ measurements of specific humidity, temperature, CO, O_3, and winds, as well as cloud-top radiation temperature and shortwave solar radiation, show substantial horizontal variability in the vicinity of the trough as a result of the sloping layers of varying properties that intersect the boundary layer.

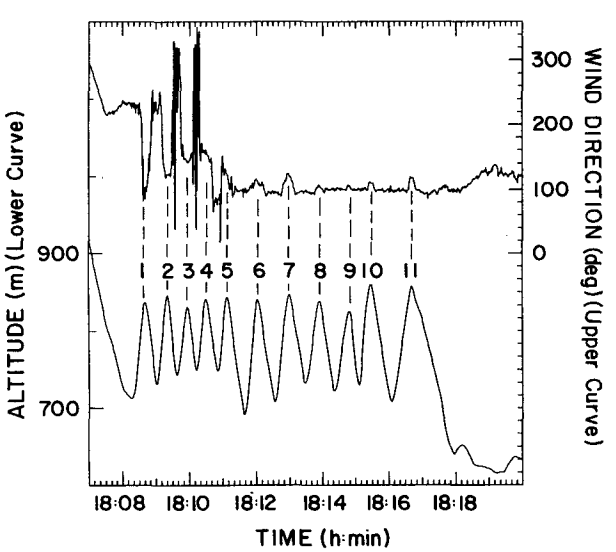

FIG. 7(g). As in Fig. 7(a) except with wind direction.

This complicates the analysis of observations from stratocumulus field studies, since typically horizontal homogeneity is assumed. The analysis here provides a specific example to support the conclusions of Kawa and Pearson (1989a,b), who also found large horizontal gradients in the jump of ozone across the boundary-layer top and large vertical gradients in ozone and humidity profiles above the boundary layer in the same region and at the same time of year.

It has been argued (e.g., Albrecht 1989) that increased aerosol concentrations, or more specifically, increased cloud condensation nuclei (CCN) can alter the stratocumulus cloud cover and its reflectivity. For the same amount of liquid water, increasing the CCN would reduce the cloud droplet size, increase the cloud reflectivity, and reduce the drizzle rate. Reducing the drizzle rate would tend to preserve the cloud and make it less likely to break up. Our results show a ~30% decrease in average cloud droplet diameter below the aerosol layer, but reduced liquid water in the vicinity of the intersection zone. However, this is a region of large horizontal variability, so that other effects may be important. For example, both the low Richardson number and the larger boundary-layer ozone values in the region of intersection indicate that the entrainment rate may be larger there.

Paluch et al. (1989) discuss data from this same flight. They suggest that the high ozone layer starting just above the inversion is a baroclinic flow of polluted, ozone-rich air from the Los Angeles area, driven by the temperature contrast between the relatively warm continental boundary-layer air heated by solar radiation, and the cool marine air over the ocean. We suggest that this also is the source of the particle-laden air observed with the NAILS. The observed wind direction, both above and below cloud is certainly consistent with a continental origin. The schematic illustration of baroclinic flow from Paluch et al. (1989) serves as background on a much larger spatial scale for our Figs. 2 and 6.

Because of its ability to reveal vertical cross sections of aerosol distributions, we have shown that the NAILS is a unique and important tool in studying the relationship between structure in the free atmosphere and its interaction with the boundary layer when combined with in situ observations of the remotely-sensed structures.

Acknowledgments. We are grateful to NCAR pilots J. Tejcek and H. Boynton for observing and reporting the quasi-linear trough that provided the basis for the further analysis reported here. I. R. Paluch provided

many useful insights into the analysis and interpretation of the aircraft data. We also thank the reviewers for their helpful comments. Part of this work was supported by the Office of Naval Research under Interagency Agreement (IA) No. 89–12.

REFERENCES

Albrecht, B. A., 1989: Aerosols, cloud microphysics, and fractional cloudiness. *Science,* **245,** 1227–1230.

——, D. A. Randall and S. Nicholls, 1988: Observations of marine stratocumulus clouds during FIRE. *Bull. Amer. Meteor. Soc.,* **69,** 618–626.

Boers, R., J. D. Spinhirne and W. D. Hart, 1988: Lidar observations of the fine-scale variability of marine stratocumulus clouds. *J. Appl. Meteor.,* **27,** 797–810.

Browell, E. V., A. F. Carter, S. T. Shipley, R. J. Allen, C. F. Butler, M. N. Mayo, J. H. Siviter, Jr. and W. M. Hall, 1983: NASA multipurpose airborne DIAL system and measurements of ozone and aerosol profiles. *Appl. Opt.,* **22,** 522–534.

Kawa, S. R., and R. Pearson, Jr., 1989a: Ozone budgets from the Dynamics and Chemistry of Marine Stratocumulus Experiment. *J. Geophys. Res.,* **94,** 9809–9817.

——, and ——, 1989b: An observational study of stratocumulus entrainment and thermodynamics. *J. Atmos. Sci.,* **46,** 2649–2661.

Melfi, S. H., J. D. Spinhirne, S.-H. Chou and S. P. Palm, 1985: Lidar observations of vertically organized convection in the planetary boundary layer over the ocean. *J. Climate Appl. Meteor.,* **24,** 806–821.

Paluch, I. R., D. H. Lenschow and R. Pearson, Jr., 1989: Ozone as a tracer of mixing in the marine boundary layer. *Proceedings Symposium on the Role of Clouds* in *Atmospheric Chemistry and Global Climate,* Anaheim, Amer. Meteor. Soc., 239–244.

Post, M. J., 1978: Experimental measurements of atmospheric aerosol inhomogeneities. *Opt. Lett.,* **2,** 166–168.

Radke, L., J. A. Coakley, Jr. and M. D. King, 1989: Direct and remote sensing observations of the effects of ships on clouds. *Science,* **246,** 1146–1149.

Schwiesow, R. L., 1987: The NCAR airborne infrared lidar system (NAILS), design and operation. NCAR Technical Note 291+1A, June, 1987, 38 pp. [Available from NCAR, P.O. Box 3000, Boulder, CO 80307.]

——, V. M. Glover and D. H. Lenschow, 1988: Measurements with airborne lidar: an example from FIRE and potential applications to turbulence and diffusion. Preprint Volume, *Eighth Symposium on Turbulence and Diffusion,* San Diego, Amer. Meteor. Soc., 197–200.

Uthe, E. E., N. B. Nielsen and W. L. Jimison, 1980: Airborne Lidar Plume and Haze Analyzer (ALPHA-1). *Bull. Amer. Meteor. Soc.,* **61,** 1035–1043.